Engineering Structures 286 (2023) 116116

Contents lists available at ScienceDirect

Engineering Structures

journal homepage: www.elsevier.com/locate/engstruct

A local response function approach for the stress investigation of a centenarian steel railway bridge

Alessandro Menghini [a,*], John Leander [b], Carlo Andrea Castiglioni [a]

[a] Politecnico di Milano, Department of Architecture, Built Environment and Construction Engineering, Piazza Leonardo da Vinci 32, Milan, 20133, Italy
[b] KTH Royal Institute of Technology, Department of Civil and Architectural Engineering, Brinellvägen 23, Stockholm, 100 44, Sweden

ARTICLE INFO

Keywords:
Surrogate model
Monitoring
Bridge assessment
Time-dependent damage
Stress histories

ABSTRACT

Local stress concentrations in some specific geometric details often play an essential role in time-dependent damage propagation. However, measured strain or stress data are generally available in locations that are not the most critical ones. Proper numerical models are thus required to aid the damage severity assessment. In this paper, a surrogate model procedure based on the local response function method is proposed to accurately predict stress time histories in particular regions of bridges through a multiscale numerical analysis. The methodology is calibrated on the basis of direct strain measurements on a railway bridge in Vänersborg, Sweden. The bridge is currently monitored with a set of strain gauges, accelerometers, and an inclinometer allowing the investigation of its in-service conditions during the train passages and the lifting of the bascule truss. The results show the reliability of the method for stress prediction in specific regions of the bridge without the availability of directly measured data together with more detailed knowledge about the stress histories that could lead to fatigue or corrosion damage.

1. Introduction

A huge number of steel infrastructures were built during the 20th century due to the rapid development of the transport system. Nowadays, the average in-service life of those bridges is about 100 years. Consequently, many of these structures show some damage or weakness signals due to time-dependent phenomena (i.e. fatigue, corrosion). Moreover, due to increasing traffic demands, these structures are subjected to load volumes and frequencies higher than those for which they were originally designed. Therefore, an enhanced assessment of their actual in-service behaviour is required. Using sensors to measure strain has been proven beneficial to estimate better the in-service load effect as well as to reduce their uncertainties [1–4]. However, measured strain or stress data are generally available in specific locations that are not the most critical ones. Indeed, sensors are commonly placed in positions away from areas affected by geometric stress concentrations. Proper regression models are thus required to aid the stress distribution investigation. Local stress concentrations in specific geometric details often play an essential role in time-dependent damage propagation [4].

Recently, enhancements in stress histories computation have been made through model/experimental-based procedures in the context of fatigue damage computation.

Leander [5] compared the uses of theoretical influence lines and an artificial neural network (ANN) method to predict the stress time history response from train passages, the trained networks were used to predict the response at different bridge parts starting from the response measured with sensors as input. Results showed that, as long as the input variables are similar in terms of time variance, accurate stress time history predictions can be reached with artificial neural networks. Other artificial neural network applications can be found in [6] by the use of dynamic load test data for predicting the static behaviour of the bridge. Further studies related to the influence lines methods for the prediction of stress time-history can be found in [7,8].

Horas et al. [9–11] studied crack initiation with the modal superposition technique with an application to the Varzeas Bridge case study. In those cases, after defining the modal quantities for bridge modes, the modal coordinates' time histories are calculated. Stresses and strains are thus derived by superimposing a limited number of vibration modes. Moreover, the modal superposition technique was also used by Albuquerque et al. [12,13] for the stress intensity factors computation of a propagating crack. In these studies, a multi-scale procedure is used in which the modal displacement fields of a global model are exported as the submodel nodes' boundary conditions [9–11,14].

Nabuco et al. [15,16] derived the stress history for the fatigue analysis of an offshore tripod jacket platform using the modal expansion techniques. Investigations have been carried out on scale models as well as a full scale one, by considering the operational loads as well

* Corresponding author.
E-mail address: alessandro.menghini@polimi.it (A. Menghini).

https://doi.org/10.1016/j.engstruct.2023.116116
Received 24 November 2022; Received in revised form 28 March 2023; Accepted 4 April 2023
Available online 12 April 2023
0141-0296/© 2023 The Authors. Published by Elsevier Ltd. This is an open access article under the CC BY license (http://creativecommons.org/licenses/by/4.0/).

as random vibrations. Tarpø et al. [17] compared the modal expansion techniques by using expanded experimental mode shapes and finite element mode shapes.

Tchemodanova et al. [18,19] applied the Kalman filtering for model and data fusion combined with a sub-structuring approach for the strain time history estimation at not-instrumented locations. In particular, in [18], strain estimates generated via Modal Expansion are enhanced into an augmented Kalman Filter (AKF) as virtual measurements. The investigations are applied to the detail of a rollercoaster connection subjected to operational multiaxial non-proportional loading. Other uses of the Kalman Filter for stress estimation can be found in [20–22], and for Modal expansion [23,24].

Generally, the main difficulties encountered by these complex approaches are related to their application when the problem is affected by high-level uncertainty (i.e. complex geometric features or loading conditions affecting the systems). This paper thus proposes a fast-running method that can accurately predict experimental stress time histories at locations distant from those monitored, without the need for knowledge of the actual loading conditions such as axle loads and distances.

In this paper, a surrogate model-based procedure based on the response function method is presented. This procedure combines multiscale numerical models with experimental strains from monitored locations to predict the stress range in different bridge parts under in-service loading conditions. The procedure takes into account load sequence and interaction, which are often ignored [25,26] and are key factors in determining time-dependent damage, such as that caused by fatigue or corrosion fatigue. This paper implemented a methodology for fatigue damage evaluation using the rain flow counting method to calculate stress range spectra for the application of the S-N curve method (stress range versus number of cycles to failure for the linear accumulation of fatigue damage) [27–29]. Additionally, the approach has been used to investigate the stress caused by a specific detail characterized by corrosion phenomena, with the aim of analysing its theoretical stress sensitivity to damage severity.

The methodology is calibrated based on direct strain measurements on a railway bridge in Vänersborg, Sweden. The bridge, inaugurated in 1914, is an openable bascule bridge constructed by riveted steel members. The bridge is currently monitored with a set of strain gauges, accelerometers, and an inclinometer allowing the investigation of its in-service conditions during the train passages and the lifting of the bascule truss. The results obtained in terms of the stress histories demonstrate the capability of this method in identifying damage features in locations remote from the monitored locations and predicting the reliable range and number of stress cycles for fatigue damage assessment. This can be beneficial for bridge monitoring and management operations.

2. Stress computation methodology: local response function approach

The response function method consists in approximating a complex implicit relationship between a response and controllable variables using a polynomial formulation. This procedure is generally used in structural optimization [30–33] and reliability analysis [34–36]. In this paper, the methodology is used to derive the correlation between local principal stress time histories at different locations. The main methodology for the local response function application is depicted in Fig. 1 and consists in fitting the local sampled stress data by a least-square regression technique. This research procedure employs a multiscale numerical analysis approach wherein a global model is used to evaluate the overall numerical displacements of the bridge when exposed to railway loadings, and refined local models are employed to provide a more detailed analysis of stress concentration effects and the primary stress distribution. The global displacements at the beam nodes (DOFs) are then exported to local models and used as boundary conditions (BCs) in the master nodes of the refined solid formulation to investigate the stress time histories and their associated response functions. Assuming that the numerical models are accurate and consistent with direct measurements, the approximated response function can be employed to estimate the experimental response function at locations that are not being monitored, as illustrated in Fig. 1.

According to the response function method, a general system response $\hat{\sigma}$ depends on the controllable input variables $\sigma_1, \sigma_2, ..\sigma_k$, as:

$$\hat{\sigma}(x) = f\left(\sigma_1, \sigma_2, ..\sigma_k\right) + \epsilon \tag{1}$$

where f is the form of response function approximating a complex implicit relationship between a response and controllable variables, and ϵ is the variability error not accounted for in f [30]. In particular, given two local stress components σ_1 and σ_2 located in two different locations of the bridge, if an experimental correlation between these two quantities can be identified, it is possible to express their correlation f through proper approximated polynomials envelope of grade n. Thus, the stress σ_1 at each jth time step can be expressed:

$$\sigma_{1j}\left(\sigma_{2j}\right) = \beta_0 + \beta_1\sigma_{2j} + \beta_2{\sigma_{2j}}^2 + \beta_3{\sigma_{2j}}^3 + \cdots + \beta_n{\sigma_{2j}}^n \tag{2}$$

with $\beta_0, \beta_1, \beta_2, \beta_3, ..\beta_n$ that are the $m = (n+1)$ unknown coefficients to be determined. In this work, a third-order cubic expression of the response function is used as illustrated in Appendix for the stress history prediction. Let β be the column vector containing the unknown coefficients for each jth response parameter. The least-square estimator of β can be written as [37,38]:

$$\beta = \left(\mathbf{U}^T\mathbf{U}\right)^{-1}\mathbf{U}^T\sigma_{1j} \tag{3}$$

where $\mathbf{U}$ is a $N \times m$ matrix collecting parameters for each jth time step in the cubic form in the training population and N is the total number of considered jth time steps in the stress time variant spectrum. $\mathbf{U}$ matrix can be expressed as:

$$\mathbf{U} = \begin{bmatrix} 1 & \sigma_{2j} & \left(\sigma_{2j}\right)^2 & \left(\sigma_{2j}\right)^3 & \dots & \left(\sigma_{2j}\right)^n \\ \vdots & \vdots & \vdots & \vdots & \ddots & \vdots \\ 1 & \sigma_{2N} & \left(\sigma_{2N}\right)^2 & \left(\sigma_{2N}\right)^3 & \dots & \left(\sigma_{2N}\right)^n \end{bmatrix} \tag{4}$$

The approximated response $\hat{\sigma_{1j}}$ at any untried σ_{2j} can be finally computed with Eq. (2). Provided that the numerical models are reliable and show agreement with direct measurements at the same locations S_1, S_2, the approximated response function f (such that $S_{1j} = f\left(S_{2j}\right)$) would approximate the exact relationship between the actual measured parameters. The estimated approximation of $\hat{S}_1$ is then expressed:

$$\hat{S}_1\left(S_2\right) = f\left(S_2\right) + \epsilon \tag{5}$$

where ϵ is the random error which is commonly assumed to be normally distributed with zero mean and variance σ^2. The error at each observation is considered to be independent and identically distributed. More in general, the methodology allows the estimation of the stress history at specific locations S_j, giving the experimental output at another location, considering the least square estimator computed with an advanced numerical model of the structure, providing a higher numerical correlation between the two parameters.

3. The Vänersborg bridge

3.1. The bridge geometry and main characteristics

The bridge was built by the J. Gollnow & Sohn Company between 1914–1916 over Trollhätte Kanal in Vänersborg, in the southwest of Sweden. The bridge has the design of a heel trunnion bascule, sometimes called a Strauss bascule, with a movable leaf made as a riveted truss and a concrete counterweight. The bridge geometry is shown in Fig. 2. The bridge has an overall length of about 68 m with a truss main span length and height equal to 42 m and 7.6 m, respectively.

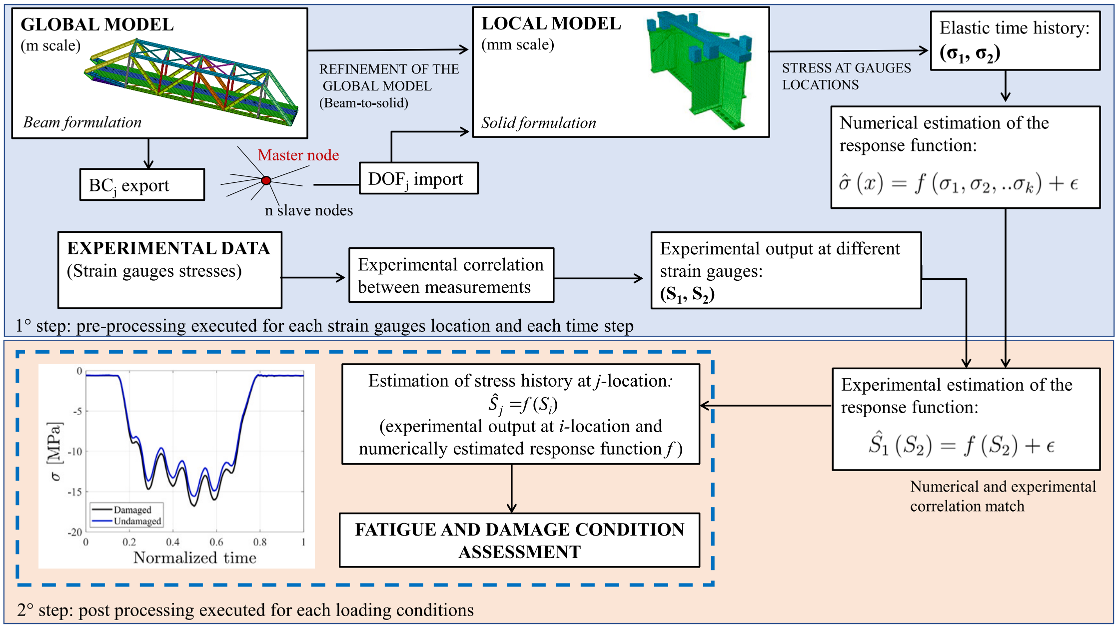

Fig. 1. Investigation methodology flowchart.

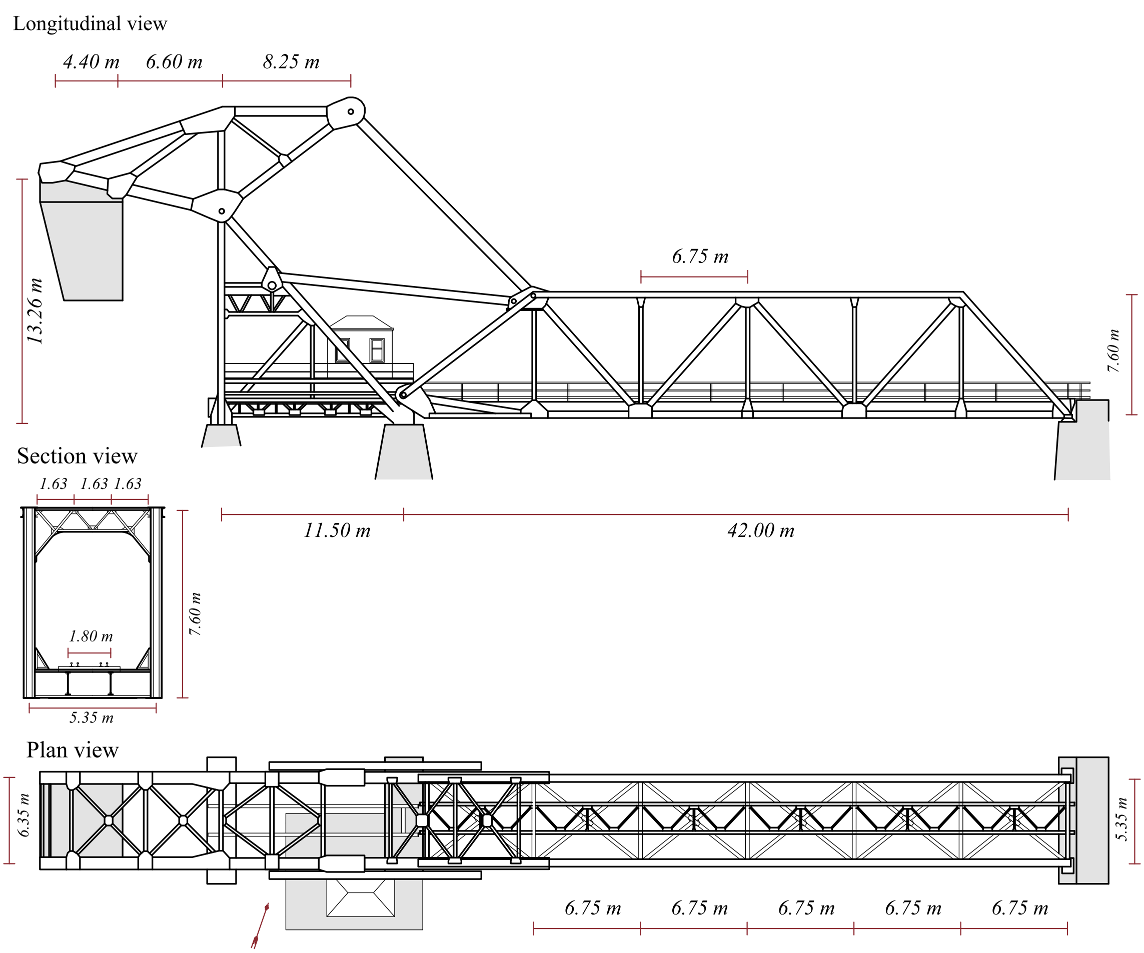

Fig. 2. Vänersborg bridge geometry, plan view and longitudinal view.

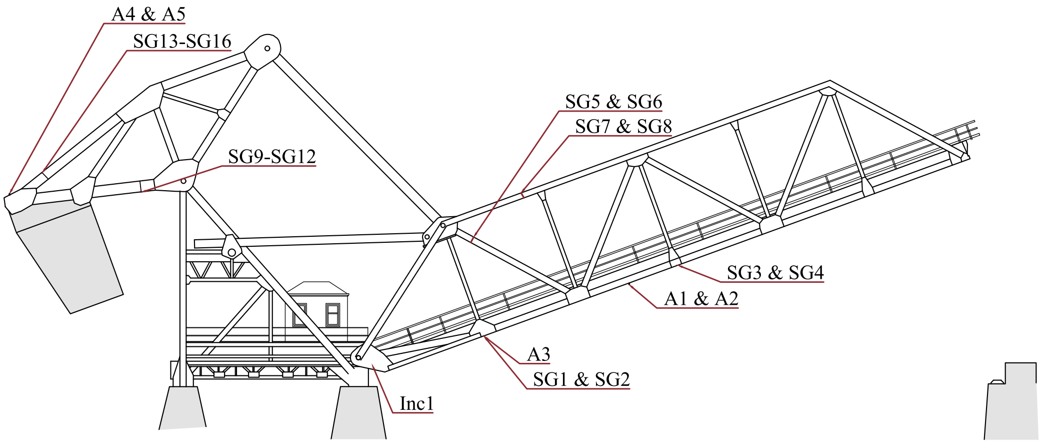

Fig. 3. Monitoring layout for the Vänersborg bridge.

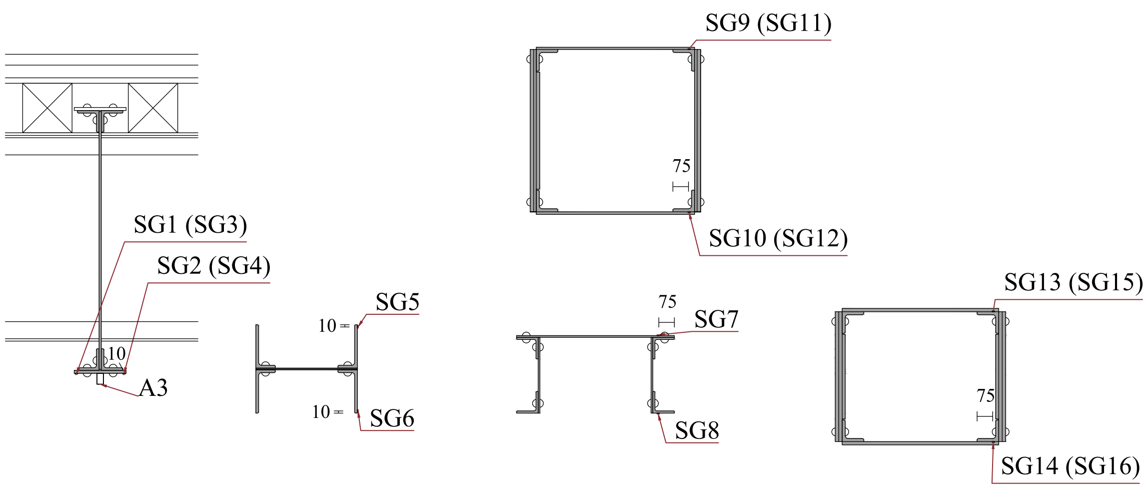

Fig. 4. Strain gauges detailed locations.

(a) Inclinometer placed at bridge support.

(b) Strain gauges placed at bottom flanges of the main crossbeams.

Fig. 5. Experimental placement of sensors.

The single-leaf trunnions, allowing the bascule span's lifting, are connected to a fixed support by thick steel plates anchored to a concrete pier. The bridge is simply supported on the other side. The bridge's lower deck is composed of steel members built up by riveted plates and L profiles. The lower chords of the truss have box-like sections, while crossbeams and stringers have I sections. Diagonal horizontal bracings are placed between the chords and the stringer beams. The verticals and diagonals in the truss have built-up I sections. The upper chords have box sections laterally braced by transversal trusses consisting of L profiles, as shown in Fig. 2.

3.2. Experimental campaign

The bridge is monitored to assess its actual bearing capacity and its in-service internal stresses. The instrumentation of the bridge involves 16 uniaxial strain gauges, 5 uniaxial accelerometers, and an inclinometer to control the lifting of the bascule truss, as illustrated in

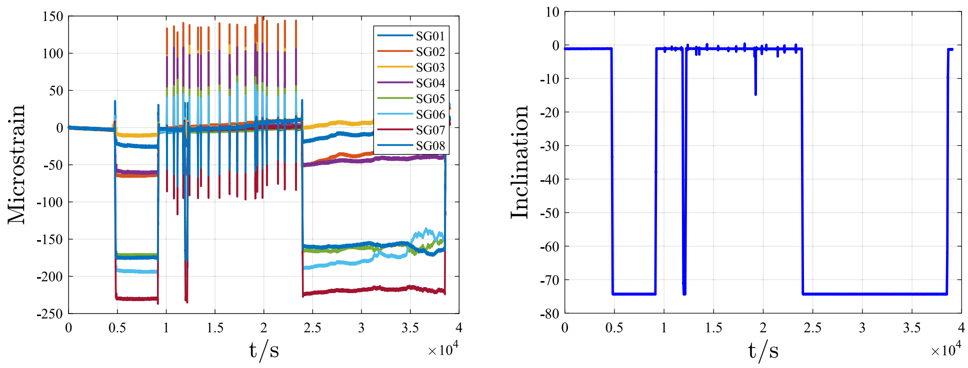

(a) Strain gauges output. **(b)** Inclinometer output.

Fig. 6. Experimental data output for activities for 11/24 h.

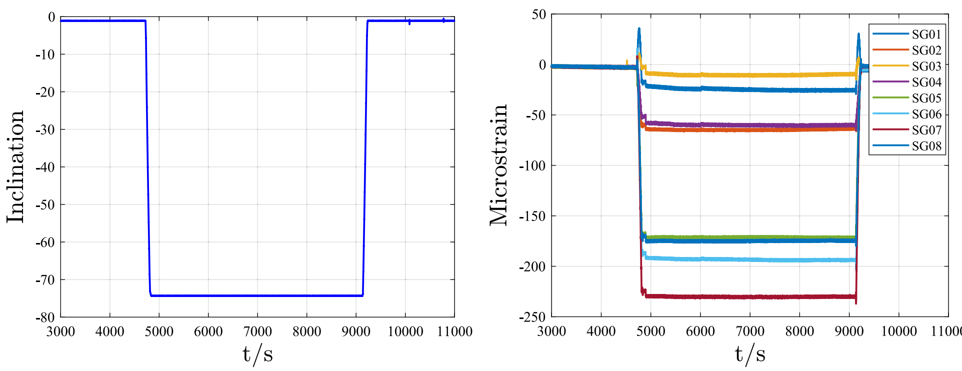

(a) Inclination degree. **(b)** Measured strain.

Fig. 7. Experimental data output due to the lifting of the bascule truss.

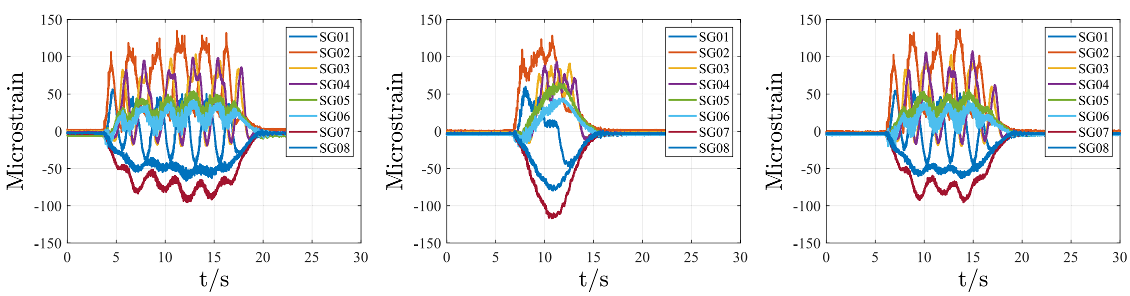

(a) Train n.1. **(b)** Train n.2. **(c)** Train n.3

Fig. 8. Microstrain measurements at strain gauges locations (SG1-8).

Fig. 3. The bridge is continuously monitored and raw data are stored in terms of 10 min events and stored by an on-site acquisition system. Data is reached and visualized through the IoTBridge®cloud-based solution. Strain gauges are located in order to measure nominal strains at positions away from possible geometrical stress concentrations (Fig. 4).

Strain gauge locations are decided based on visual inspections as well as preliminary computations. Photographs of the installed strain gauges (SG1-2) and the inclinometer are shown in Fig. 5.

The gauges are placed on the crossbeams (SG1-2 and SG3-4), on the diagonal (SG5-6), on the truss upper chord (SG7-8) and 8 gauges (SG9-16) are located on the bridge counterweight. A typical sensor output is shown in Fig. 6 for a single-day experimental activity in terms of measured strain and registered rotation with the inclinometer. Figs. 7 and 8 illustrate the experimental data gathered during the lifting of the bascule truss and the passages of three different train types as examples.

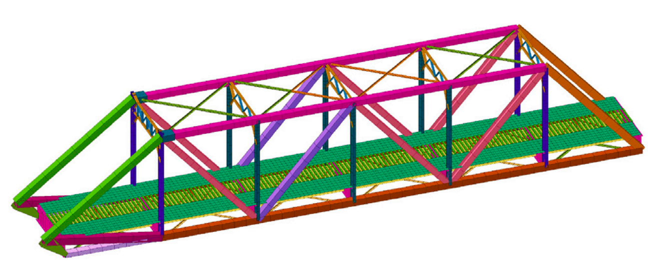

Fig. 9. Global numerical model of the Vänersborg bridge.

4. Numerical modelling procedures

This research procedure involves an advanced multiscale numerical analysis (Fig. 1) that links a global model and separate substructures of

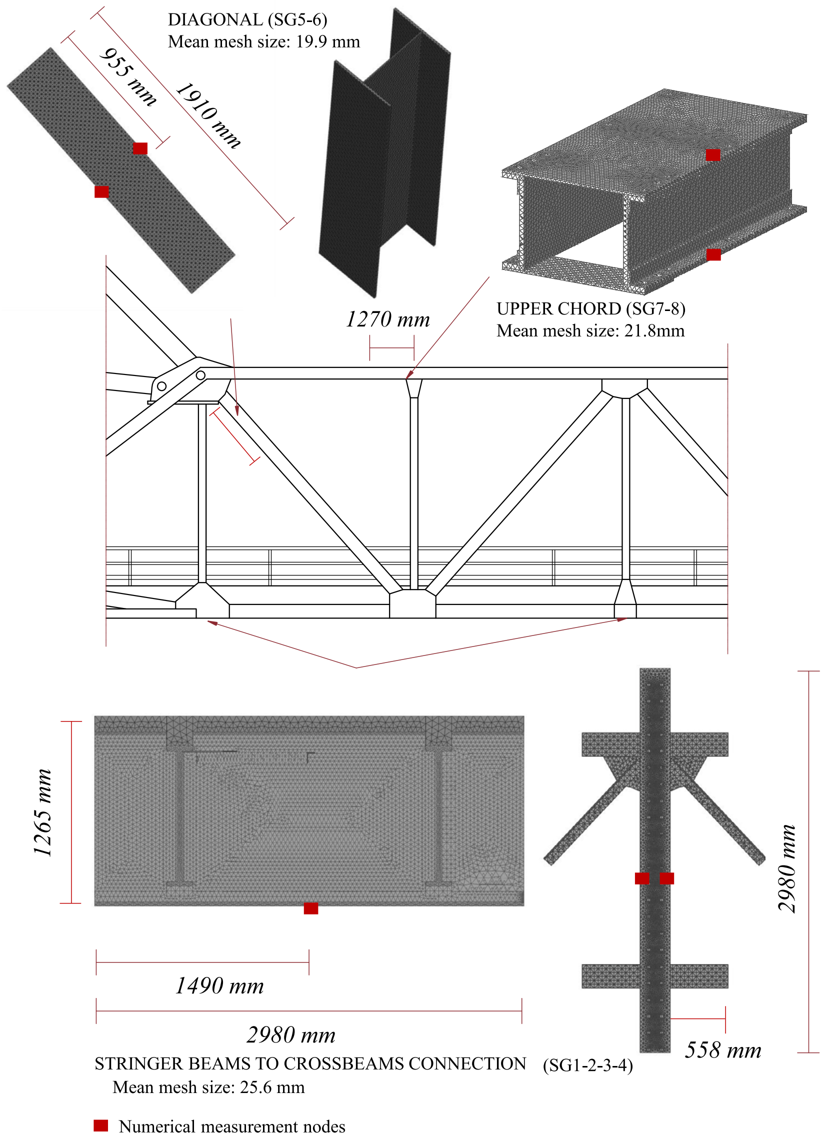

Fig. 10. Local substructure models of the Vänersborg bridge and their locations.

the bridge through displacement fields. The model updating approach is used to appraise the global numerical model, reducing uncertainties in the problem by measuring strain at each strain gauge during the lifting of the bascule truss. Once calibrated, the global model predicts the displacements resulting from the passage of a typical Regina X55 train, and the refined submodels are used to derive the stress time-histories.

4.1. Global modelling

A global numerical model of the bridge truss has been developed with MIDAS®software [39] (Fig. 9). The global numerical model is carried out with beam elements (main stinger beams, diagonals, cross-beams, and bracings). Shell elements are used to model the wooden planks connected to the main crossbeams through rigid translational links. Ballastless railway tracks, such as rails and wooden sleepers, are modelled with beam elements connected with the bridge grid. The wooden sleepers transfer the traffic loads to the stringers and crossbeams. The geometric characteristics are, where possible, taken from original design drawings. Concerning the representation of the bearings, they are modelled as fixed translational constraints on the trunnion side, as rollers on the opposite side, allowing longitudinal translations. For the main structural elements, steel grade S275 is considered, defined by elastic modulus $E = 210$ GPa, Poisson's ratio $\nu = 0.3$ and mass density $\rho = 7850$ kg/m^3. Riveted connections' elastic modulus is assumed equal to $E_r = 199$ GPa [11,40]. Sleepers have wooden material properties ($E_w = 14$ GPa, $\rho_w = 1020$ kg/m^3, $\nu_w = 0.2$). The truss structure of the counter-weight system is not considered in the FEM formulation of this paper as it is supposed to be a statically determined independent structure, maintaining the structure in equilibrium conditions without affecting its static behaviour in the horizontal configuration.

4.2. Local modelling

Local submodels are required to investigate the behaviour in terms of local principal stress values. Solid elements submodels are carried

(a) Reference configuration. (b) Lifting configuration.

Fig. 11. Bridge's lifting of the bascule truss. Photographs from the publicly available digital records of Vänersborg's Museum.

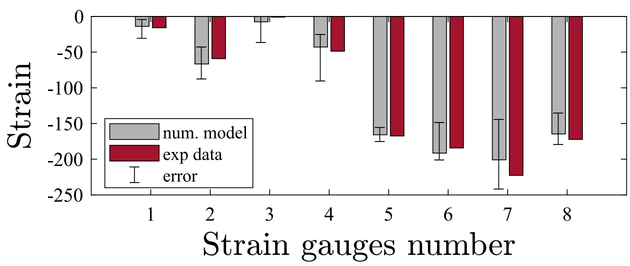

Fig. 12. Numerical principal and experimental strain comparison after the model updating procedure.

out, and the local geometrical properties (i.e. dimensions and thicknesses) are assessed following the available design drawings as well as visual surveys. The connections between the local submodel to the global beam model are obtained through master nodes to which the displacements (D_x, D_y, D_z, R_x, R_y, R_z) of the global beams model are assigned. The master nodes are connected with the edge extreme nodes through infinite rigid links in the three rotations and the three translations. In Fig. 10, the local submodels developed with Midas FEA NX®software [39] are described.

In particular, the model substructures involve the connection between the stringer beams, the crossbeams, and the floor deck diagonals. The second submodel is related to the tension diagonal where SG5-6 are located for an overall length of about 1.91 m from the gusset plate connection. The fourth substructure involves the upper chord (SG7-8 locations) for a length equal to 1.27 from the connection to the second vertical. The mesh is defined by a combination of 5-nodes pentahedrons, 8-node hexahedrons, and tetrahedrons with mean element size according to Fig. 10. Contact between parts (e.g. plates, girders, angles) is modelled as linear contact in which surfaces are not allowed to separate, and all the connected nodes have displacements associated with their compatibility conditions. Riveted connections are modelled only in the proximity of numerical measurement nodes in order to increase the computational efficiency of the numerical model. This hypothesis is made according to [11], in fact, considering the small displacement domain in civil engineering structures, the local effects of the riveted clamping force will not influence the local behaviour of stresses where strain gauges are put far from the riveted locations.

4.3. Model calibration: the lifting of the bascule truss

The local model calibration is carried out in terms of measured strains at strain gauges 1–8 after the complete lifting of the bascule truss, as depicted in Fig. 11. The final inclination reached by the truss system is equal to 75° (Fig. 7). During the lifting, the bridge's boundary conditions change, in fact in the reference configuration, the bridge is considered simply supported in its extremities. When the lifting system is activated, the truss becomes clamped due to the restraints caused by the trunnions and the link to the counterweight system. Consequently, the measured values of strain are obtained considering the difference between the strain in the final configuration and those in the initial state. The calibration analysis is carried out according to the multi-level detailing approach (Fig. 1). In particular, the displacements of the initial configuration caused by the self-weight of the bridge were calculated and derived in the local submodel using the multi-scale approach. The same procedure was repeated for the final inclined configurations. Local submodels allow the identification of the principal strain related to the position of strain gauges in the numerical model for the two configurations. The strain values are obtained from the difference between the values in the final configuration (inclination of the bascule truss) and the initial ones (horizontal configuration).

The model updating procedures are carried out considering the main uncertainty structural parameter in the numerical global model which is the lateral deck weight density ρ. Indeed, although the original design drawings showed the presence of wooden planks, recent visual inspections had revealed the presence of a steel layer upon that wooden deck. Moreover, the mass correction may also include unintentionally neglected structural parts. According to the Douglas-Reid approach [41], the dependence between the measured strain at each ith locations ϵ_i (response parameter) and the uncertain structural parameters ρ can be expressed as:

$$\epsilon_i^*(\rho) = A_i\rho + B_i\rho^2 + C_i \tag{6}$$

where ϵ_i^* is the approximation of the ith strain measure of the finite element model. The coefficients A_i, B_i, and C_i are computed for each approximated strain measure before the comparison with the experimental one. In this context, the base value of the structural parameter is assumed to be equal to $\rho^B = 3000\ \mathrm{kg/m^3}$ and an upper bound and lower bound limits for the parameter $\rho^L = 1020\ \mathrm{kg/m^3}$ (timber material), $\rho^U = 7850\ \mathrm{kg/m^3}$ (steel material) are defined, such that: $\rho^L \le \rho^B \le \rho^U$. Consequently, the A_i, B_i, and C_i coefficients are determined by computing the ith strain location, for the $(2N+1)$ unknown according to the known conditions [42,43]. The optimal parameter value is estimated by minimizing the following error function:

$$J = \sum_{i=1}^{n}\left(\epsilon_i^{Exp} - \epsilon_i^*\right)^2 \tag{7}$$

where ϵ_i^{Exp} is the ith experimentally identified strain and ϵ_i^* is the ith polynomial approximation of the numerical strain with updated structural parameters. The model calibration at SG1-8 is shown in Fig. 12 for the optimal parameter estimates $\rho = 1600\ \mathrm{kg/m^3}$.

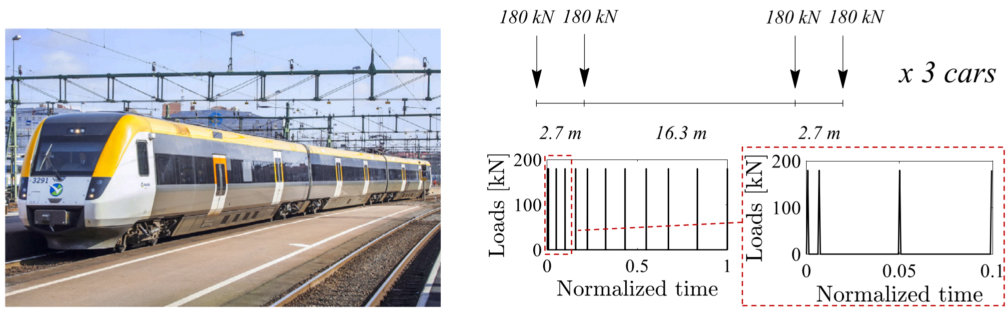

(a) Photograph of the train.

(b) Axle loads, positions and loading time-history input.

Fig. 13. Regina X55 characteristics.

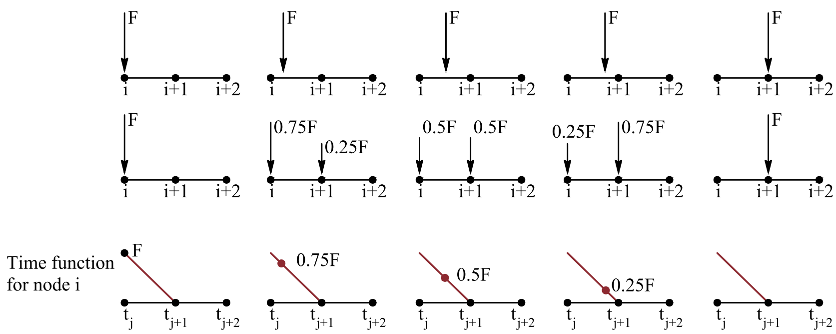

Fig. 14. Moving load to dynamic loads using time history function.

4.4. Railway loading conditions simulation

The loading conditions considered in the numerical analyses procedures correspond to an X55 Regina train, Sweden (SJ3000), from Bombardier with 3 cars. It is one of the more common trains passing through the bridge. The axle loads and corresponding positions are shown in Fig. 13.

From a numerical point of view, the traffic loading conditions are transferred from the rail nodes to wooden sleepers supported by the stringers. The load function has been applied to two bridge tracks that were spaced 1.8 m apart. Subsequently, the load is directly conveyed to the crossbeams. The load distribution is calculated based on the length of the element, the distance between the vehicle wheels, and the speed of the train. This load function is then applied to each node based on its arrival time, as illustrated in Fig. 14. The axle load is modelled as a triangular pulse load, in which the transition from node i to node $i+1$ is considered loading, while the move from node $i+1$ to node $i+2$ is regarded as unloading.

The maximum allowable velocity on the bridge is limited to 40 km/h. The dynamic loadings are applied to the FEM model of the bridge with a time history analysis with a duration equal to 50 s and a time increment equal to 0.05 s The X55 Regina axle weights are applied as time forcing functions to the bridge sleepers nodes considering a passing velocity equal to 10 km/h (Fig. 13-b). The resulting displacements and rotations for the railway passages are thus defined in Fig. 15 for two master nodes belonging to stringer beam connections to the crossbeam where SG1-SG2 are located.

5. Methodology application

Provided the reliability of the local numerical models with the experimental bridge behaviour, it is possible to express a local response function approximation if an empirical correlation exists among measurements. Subsequently, the stress response at different structure parts can be predicted based on the information of some measurement locations.

5.1. Experimental data correlation

The least-square operator β in Eq. (2) can be defined if there exists a high correlation between response and structural parameters. The correlation between stress histories at different locations is shown in Fig. 16 based on three typical train type passages experimental output. In this context, the considered train types are chosen because they represent the whole loading conditions on a typical bridge in-service day. It is possible to notice higher R-Pearson coefficient values between SG2-SG4, SG2-SG5, SG6-SG8, SG6-SG7, SG5-SG7.

However, the correlation is too low for stress history registered at SG1-SG5, SG2-SG8, SG1-SG8, showing the impossibility to establish a proper response function approximating the stress history from SG1 as controllable input or response variable. The reason for this behaviour can be due to the close locations of the strain gauge to the riveted connections, influencing locally the stress distribution. Similar behaviour is observed between data from SG2 located on the crossbeam and SG8 located on the upper chord. In this sense, the suggested surrogate model cannot be established to estimate the upper chord stress history, starting from the measured values of stress in the crossbeams in connections with the stringer beams (respectively SG1-2-3-4).

5.2. Surrogate model-based estimation of stress at different locations

Considering the master nodes displacements in the truss global model, the local principal stress history has been derived for the Regina X55 train passage according to procedures in Fig. 1. The approximate numerical response $\hat{\sigma}$ prediction obtained by the least square estimation of β (surrogate models) is shown in Fig. 17 for SG2-6 and SG5-8.

The trained least square estimators from the numerical substructure models are then used to estimate the stress response $\hat{S}$ at several locations starting from the stress measures at strain gauges locations. The experimental stress values are obtained by multiplying the experimental strains with the same elastic modulus as that of the numerical

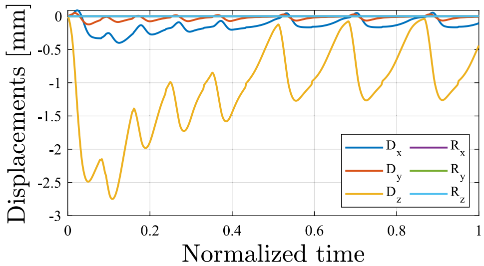

(a) Stringer beam 1.

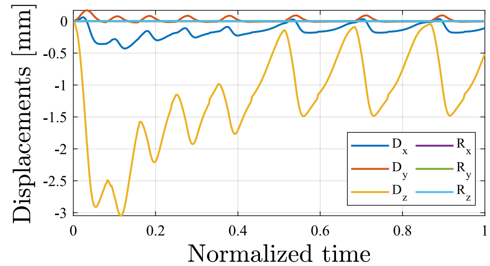

(b) Stringer beam 2.

Fig. 15. Numerical model displacements during X55 Regina train passage.

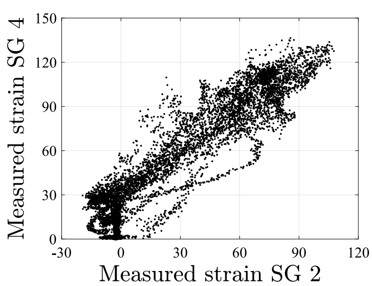

(a) SG2-SG4, R=0.9475.

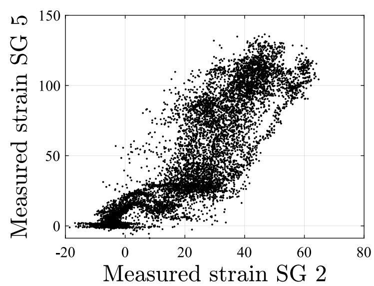

(b) SG2-SG5, R=0.9327.

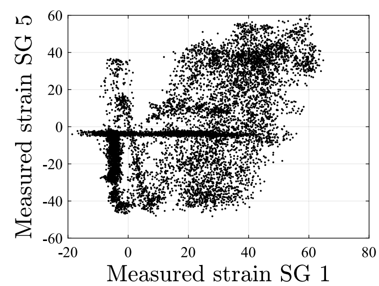

(c) SG1-SG5, R=0.5018

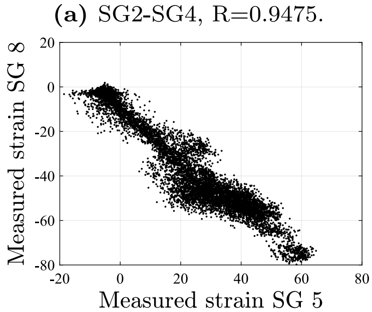

(d) SG5-SG8, R=0.9720.

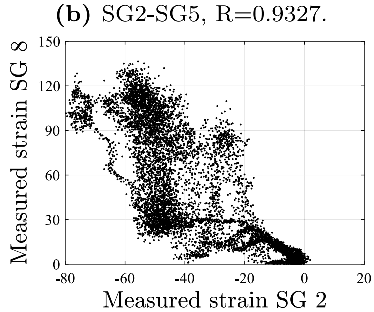

(e) SG2-SG8, R=-0.8943.

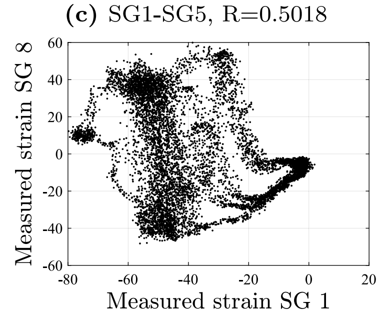

(f) SG1-SG8, R=-0.2893

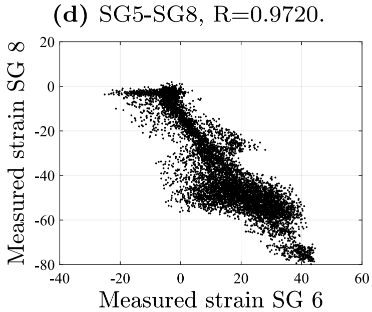

(g) SG6-SG8, R=-0.9217.

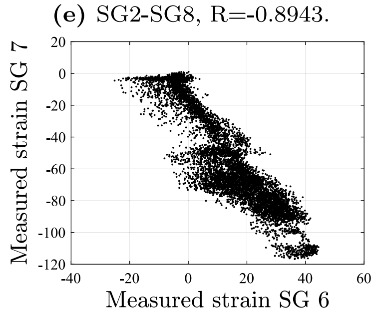

(h) SG6-SG7, R=-0.9382.

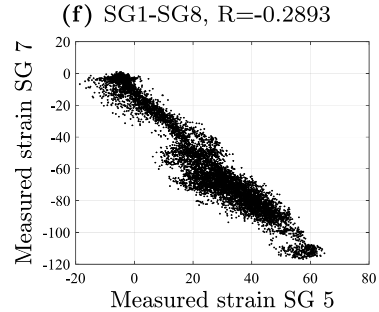

(i) SG5-SG7, R=-0.9809.

Fig. 16. Experimental measurements correlation.

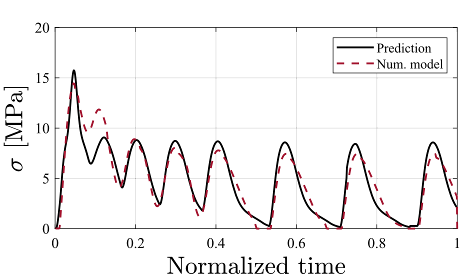

(a) $\hat{\sigma_6}(\sigma_2)$, Regina X55 train.

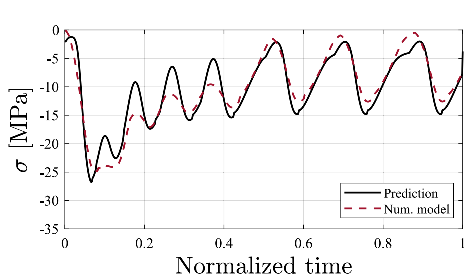

(b) $\hat{\sigma_8}(\sigma_5)$, Regina X55 train.

Fig. 17. Surrogate model numerical stress prediction.

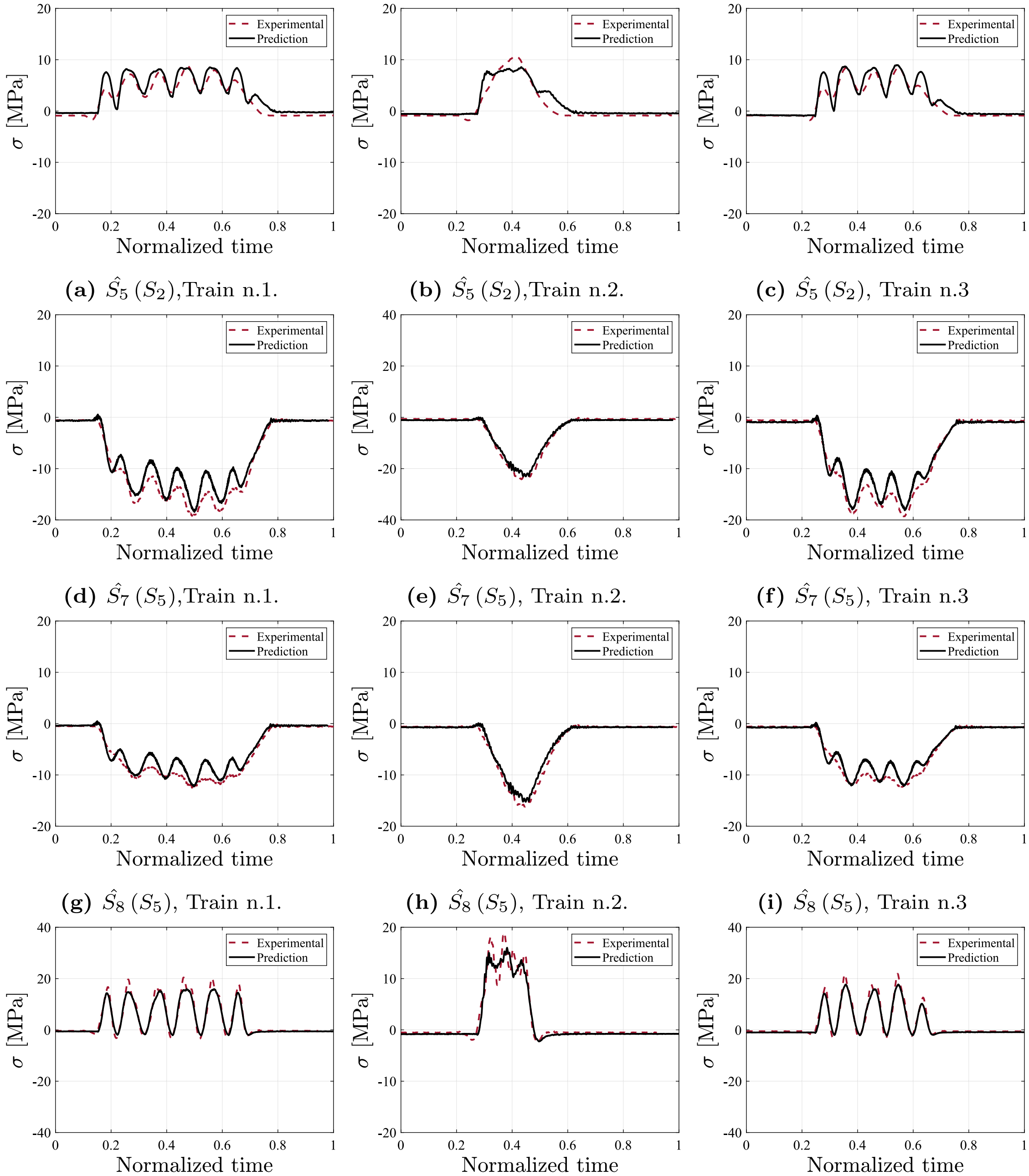

(a) $\hat{S_5}$ (S_2),Train n.1. **(b)** $\hat{S_5}$ (S_2),Train n.2. **(c)** $\hat{S_5}$ (S_2), Train n.3

(d) $\hat{S_7}$ (S_5),Train n.1. **(e)** $\hat{S_7}$ (S_5), Train n.2. **(f)** $\hat{S_7}$ (S_5), Train n.3

(g) $\hat{S_8}$ (S_5), Train n.1. **(h)** $\hat{S_8}$ (S_5), Train n.2. **(i)** $\hat{S_8}$ (S_5), Train n.3

(j) $\hat{S_4}$ (S_2), Train n.1. **(k)** $\hat{S_4}$ (S_2), Train n.2. **(l)** $\hat{S_4}$ (S_2), Train n.3

Fig. 18. Comparison of experimental and numerical stress values for several strain gauges locations.

models (E = 210 GPa). In Fig. 18, the numerical response predictions are compared with the measurements for the passages of three train types during the bridge's normal in-service conditions. The comparison between experimental and numerical stress values shows a remarkable agreement. In particular, a closer match is observed between SG5-SG7 and SG5-SG8 (Fig. 18-d-i) with respect to SG2-SG5 (Fig. 18-a-c and -j-l), this aspect is due to the lower correlation shown in Fig. 16-b between the measured strain at those locations. In the latter cases, the experimental data correlation increases their sparsity for different loading conditions on the bridge, as a consequence, the response function estimations resulted in a higher difference with respect to the experimental trends, as demonstrated in Fig. 18-b and -l.

6. Results: local damage assessment

The local response function-based methodology can be used to investigate the stress time history in specific locations prone to structural damage. With this aim, the methodology is firstly applied to study the cycle counting in a view of fatigue damage assessment with cumulative damage method approach [27]. The second application involves then the stress investigation related to a specific region of the upper chord characterized by corrosion phenomena and far away from the measurement sensors, with the aim to analyse the theoretical stress sensitivity to the damage severity.

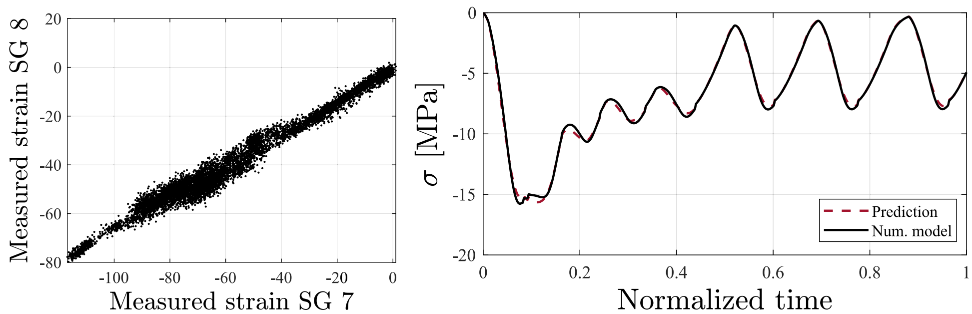

(a) Experimental correlation (R=0.9963).

(b) $\hat{\sigma_8}(\sigma_7)$, Regina X55 train.

Fig. 19. Surrogate model prediction with SG7 and SG8 data.

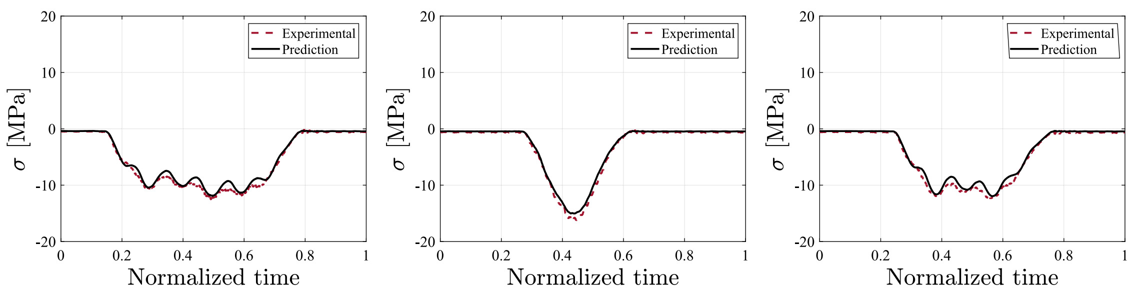

(a) $\hat{S}_8\,(S_7)$, Train n.1.

(b) $\hat{S}_8\,(S_7)$, Train n.2.

(c) $\hat{S}_8\,(S_7)$, Train n.3

Fig. 20. Comparison of experimental and numerical stress values for SG7-SG8 (submodel).

6.1. Cycle counting for fatigue damage assessment

With the objective of counting stress cycles for cumulative damage method application, stress time-history at SG7-SG8 are compared (located in the truss upper chord, as depicted in Fig. 4). Indeed, their close locations allow a higher match between the experimental and the predicted output, as shown in Figs. 19 and 20. In this case, the maximum error between experimental measurements and local response function prediction is equal to 7%.

The stress range spectra are derived from three train types loading sequences in Fig. 20. Results in Fig. 21 show that, although the experimental stress range values can slightly differ from the numerical predictions in terms of mean stress ranges, the rainflow cycle counting subroutine leads to identical results in terms of stress range spectra.

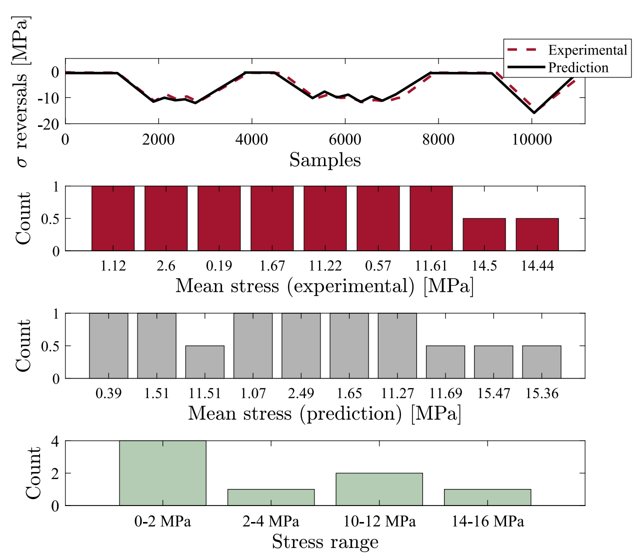

Fig. 21. Comparison of experimental and numerical average stress ranges for cycle counting algorithm.

6.2. Critical damaged location stress assessment

The local response function approach is applied to stress investigation related to the damaged detail in Fig. 22-a in the upper chord (approximately located from the connection between compression and tension diagonal, gusset plate and the vertical). The detail geometry is shown in Fig. 22-b. From a numerical point of view, in absence of direct measurements related to the damage geometry, its effects have been studied with a simulated triangular reduction of material in the upper chord's cross-section. The analysis aims to investigate the theoretical stress sensitivity to the damage features in the P1 location (Fig. 22-b).

In Fig. 23-a, the theoretical relationship between the stress prediction $\hat{\sigma}_{P1}(\sigma_7)$ obtained from SG7 output and the stress numerical history derived at position P1 is illustrated, showing a good theoretical approximate. Fig. 23-b shows the numerical prediction with response function-based surrogate models.

The actual stress history prediction at the P1 location ($\hat{S}_{P1}(S_7)$) is illustrated in Fig. 24 for the three train typologies passages, and for the bridge lifting of the bascule system during a day of in-service conditions related to the measured period.

The stress history prediction at the P1 location is then compared with the results derived for the undamaged model in Fig. 25 for the three train types passages. The stress time-history reaches a maximum difference equal to 8%, corresponding to section area reduction equal to 10% with respect to the undamaged state. These results show the theoretical stress history sensitivity to damage features and, in a more

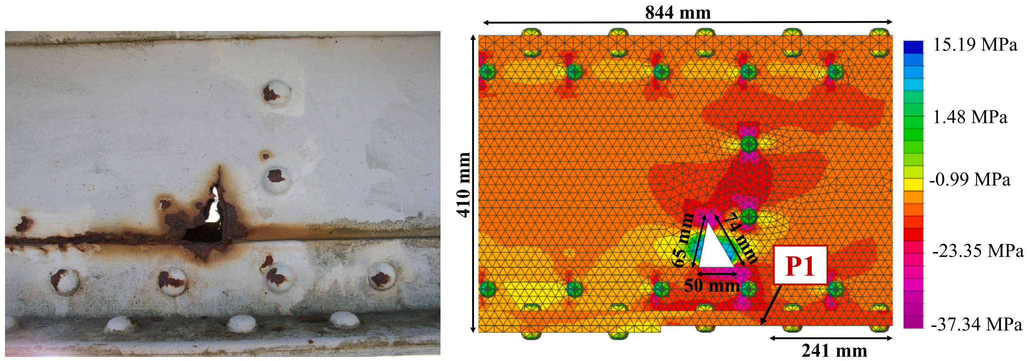

(a) Photographs of structural damage in the bridge.

(b) Numerical model detail and principal stresses.

Fig. 22. Upper chord damaged detail's geometry and definition of P1 location.

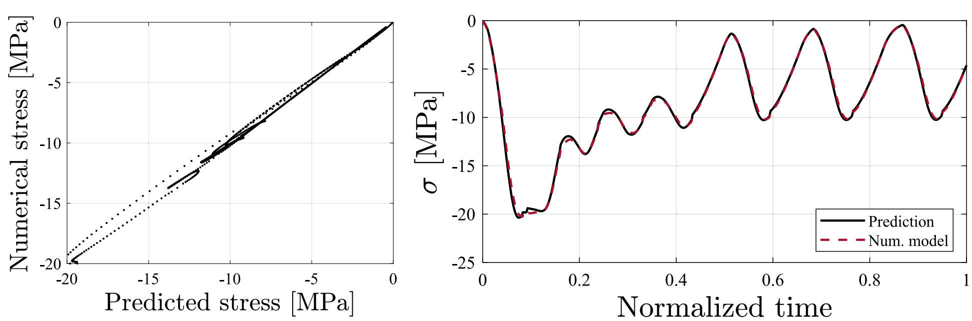

(a) Theoretical correlation.

(b) $\hat{\sigma}_{P1}(\sigma_7)$, Regina X55 train.

Fig. 23. Surrogate model prediction for the critical location.

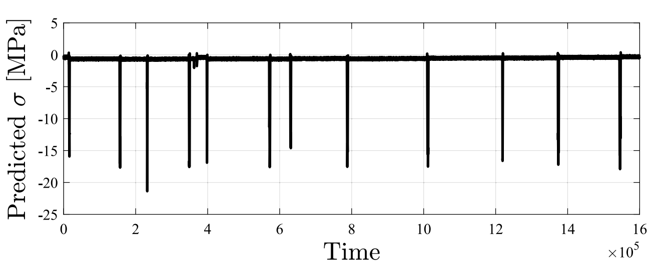

(a) $\hat{S}_{P1}(S_7)$, Train passages 11h/24.

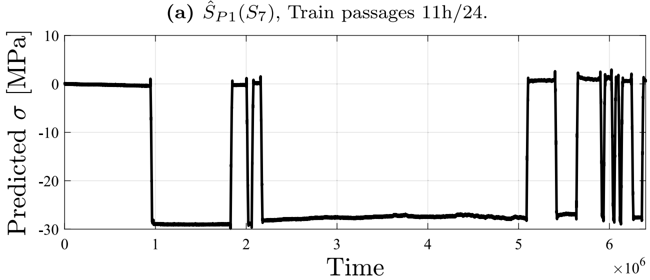

(b) $\hat{S}_{P1}$, lifting of the bascule system 24h/24.

Fig. 24. Stress time history prediction for P1 detail during in-service condition.

general sense, the possibility to monitor the damage severity by installing strain gauges at the P1 location, or by using the proposed local response function method, starting from the experimental output measured at SG7 or SG8.

7. Conclusions

In this paper, a surrogate models-based procedure based on the local response function method is presented which can predict reliable stress results in specific regions of the bridge without the availability of directly measured data at those locations and without the knowledge of the bridge's actual loading conditions. The procedure adopts a polynomial regression analysis of numerical output data to approximate the complex implicit correlation between experimental samples. This approach allows the investigation of the stress histories affecting different bridge parts that are prone to structural damage (i.e. fatigue, corrosion) during in-service loading conditions. The methodology is calibrated based on direct strain measurements on a railway bridge in Vänersborg, Sweden. The bridge, inaugurated in 1914, is an openable bascule bridge constructed by riveted steel members. The bridge was recently monitored with a set of strain gauges, accelerometers, and an inclinometer allowing the investigation of its in-service conditions during the train passages and the lifting of the bascule truss. Two main applications of the approach are finally illustrated that is the stress history estimation for cycle counting procedures for fatigue cumulative damage investigation and the stress history prediction at some damaged locations. Results show that the accuracy of the stress prediction increases significantly in cases with higher correlation. Stress time history with an error of less than 7% was predicted in the case of the bridge upper chord (R = 0.9963). The method is independent of the actual loading conditions as it was tested based on the numerical output of a typical Regina X55 train. In this sense, the approach is based on the stress domains that characterize the response and the function parameters. The method can reliably predict the stress time histories at non-instrumented locations and facilitate a more detailed knowledge of stress severity in critical or damaged parts.

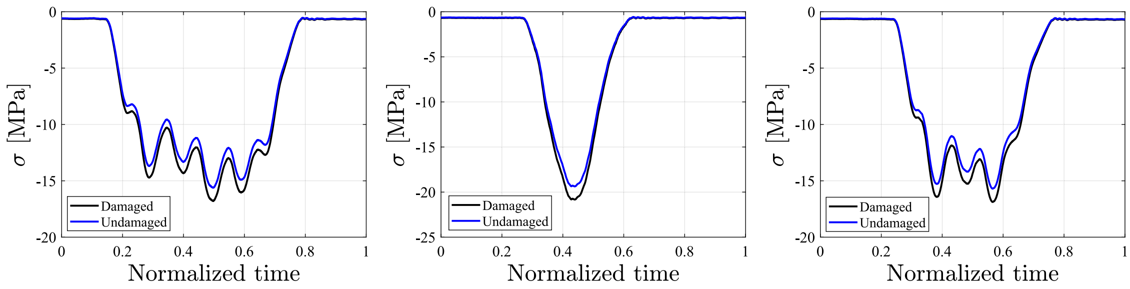

(a) $\hat{S}_{P1}(S_7)$, Train n.1. **(b)** $\hat{S}_{P1}(S_7)$, Train n.2. **(c)** $\hat{S}_{P1}(S_7)$, Train n.3

Fig. 25. Stress time history prediction for P1 detail for the damaged and undamaged model.

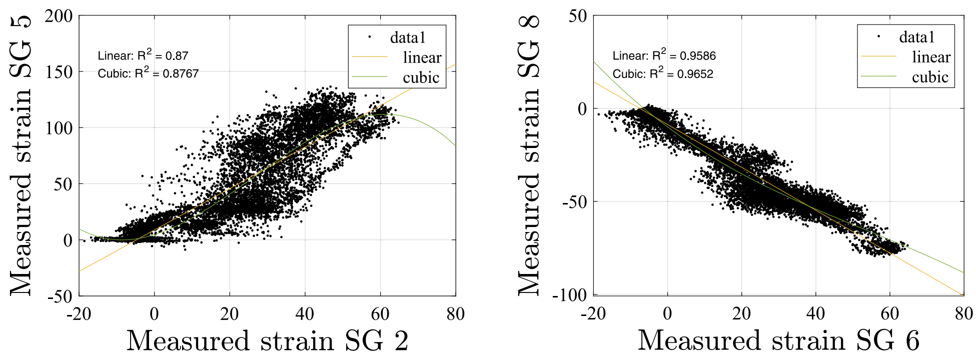

(a) SG5-SG2 regression analysis. **(b)** SG8-SG6 regression analysis.

Fig. A.26. Linear and cubic approximates of the sampled experimental data.

CRediT authorship contribution statement

Alessandro Menghini: Conceptualization, Methodology, Software, Data curation, Investigation, Writing – review & editing. **John Leander:** Methodology, Investigation, Data curation, Writing, Supervision, Review & editing, Resources. **Carlo Andrea Castiglioni:** Methodology, Investigation, Reviewing, Supervision.

Declaration of competing interest

The authors declare that they have no known competing financial interests or personal relationships that could have appeared to influence the work reported in this paper.

Data availability

Data will be made available on request

Acknowledgements

The access to the bridge document and sensor data provided by the Swedish Transport Administration (Trafikverket) and IoTBridge AB, Sweden is gratefully acknowledged. The authors want to also thank Raid Karoumi for the continuous support provided during the entire work.

Appendix. Cubic response function for stress estimation

With the aim to establish a polynomial relationship of the complex implicit relationship between stress history at different locations, a third-order polynomial expression is used in this study:

$$\sigma_{1j}\left(\sigma_{2j}\right) = \beta_0 + \beta_1\sigma_{2j} + \beta_2{\sigma_{2j}}^2 + \beta_3{\sigma_{2j}}^3 \tag{A.1}$$

The third cubic polynomial envelope is used because of the higher accuracy approximates, as shown in Fig. A.26. Indeed, higher values of the R^2 are obtained in the former case. $\beta_0, \beta_1, \beta_2, \beta_3$ in Eq. (A.1) are the 4 unknown coefficients to be determined.

The least-square estimator of β can be computed from **U** matrix (N × 4 parameters) for each jth time step in the cubic form and N is the total number of considered jth time step in the stress time history spectrum. **U** matrix takes the form:

$$\mathbf{U} = \begin{bmatrix} 1 & \sigma_{2j} & \left(\sigma_{2j}\right)^2 & \left(\sigma_{2j}\right)^3 \\ \vdots & \vdots & \vdots & \vdots \\ 1 & \sigma_{2N} & \left(\sigma_{2N}\right)^2 & \left(\sigma_{2N}\right)^3 \end{bmatrix} \tag{A.2}$$

After the $\beta_0, \beta_1, \beta_2, \beta_3$ unknown coefficients are determined, the approximated response σ_{1j} at any untried σ_{2j} can be computed with Eq. (A.1).

References

[1] Edward Zhou Y. Assessment of bridge remaining fatigue life through field strain measurement. J Bridge Eng 2006;11(6):737–44.
[2] Frangopol Dan M, Strauss Alfred, Kim Sunyong. Bridge reliability assessment based on monitoring. J Bridge Eng 2008;13(3):258–70.
[3] Caglayan BO, Ozakgul K, Tezer O. Fatigue life evaluation of a through-girder steel railway bridge. Eng Fail Anal 2009;16(3):765–74.
[4] Kühn Bertram, et al. Assessment of existing steel structures: recommendations for estimation of remaining fatigue life. In: No. BOOK. Joint Research Center; 2008.
[5] Leander John. Fatigue life prediction of steel bridges using a small scale monitoring system. TRITA-ABE-RPT-2226, 2018.
[6] Wu Ying, et al. Stress prediction of bridges using ANSYS soft and general regression neural network. Structures 2022;40. Elsevier.
[7] Leander John, Andersson Andreas, Karoumi Raid. Monitoring and enhanced fatigue evaluation of a steel railway bridge. Eng Struct 2010;32(3):854–63.
[8] Leander John. Refining the fatigue assessment procedure of existing steel bridges. TRITA-BKN-118, KTH Royal Institute of Technology; 2013, Diss..

[9] Silva Horas C, et al. Application of modal superposition technique in the fatigue analysis using local approaches. Procedia Eng 2016;160:45–52.
[10] Horas Cláudio S, De Jesus Abílio MP, Calçada Rui. Efficient progressive global-local fatigue assessment methodology for existing metallic railway bridges. J Construct Steel Res 2022;196:107431.
[11] Horas Cláudio S, et al. Efficient multiscale methodology for local stress analysis of metallic railway bridges based on modal superposition principles. Eng Fail Anal 2022;138:106391.
[12] Albuquerque C, De Castro PMST, Calçada R. Efficient crack analysis of dynamically loaded structures using a modal superposition of stress intensity factors. Eng Fract Mech 2012;93:75–91.
[13] Albuquerque Carlos, et al. An efficient methodology for fatigue damage assessment of bridge details using modal superposition of stress intensity factors. Int J Fatigue 2015;81:61–77.
[14] Kiss K, Dunai L. Stress history generation for truss bridges using multi-level models. Comput Struct 2000;78(1–3):329–39.
[15] Nabuco Bruna, et al. Reliability analysis of offshore structures using OMA based fatigue stresses. In: International conference on offshore mechanics and arctic engineering, vol. 57656. American Society of Mechanical Engineers; 2017.
[16] Nabuco Bruna, et al. Fatigue stress estimation of an offshore jacket structure based on operational modal analysis. Shock Vib 2020;2020.
[17] Tarpø Marius, et al. Expansion of experimental mode shape from operational modal analysis and virtual sensing for fatigue analysis using the modal expansion method. Int J Fatigue 2020;130:105280.
[18] Tchemodanova Sofia Puerto, et al. Remaining fatigue life prediction of a roller coaster subjected to multiaxial nonproportional loading using limited measured strain locations. In: Structures congress conference 2019. 2019.
[19] Tchemodanova Sofia Puerto, et al. State estimation for prediction of fatigue life for a rollercoaster connection subjected to operational multiaxial nonproportional loading. J Struct Eng 2021;147(5).
[20] Ren Peng, Zhou Zhi. Strain estimation of truss structures based on augmented Kalman filtering and modal expansion. Adv Mech Eng 2017;9(11):1687814017735788.
[21] Ren Peng, Zhou Zhi. Strain response estimation for the fatigue monitoring of an offshore truss structure. Pac Sci Rev 2014;16(1):29–35.
[22] Papadimitriou Costas, et al. Fatigue predictions in entire body of metallic structures from a limited number of vibration sensors using Kalman filtering. Struct Control Health Monit 2011;18(5):554–73.
[23] Skafte Anders, et al. Experimental study of strain prediction on wave induced structures using modal decomposition and quasi static Ritz vectors. Eng Struct 2017;136:261–76.
[24] Iliopoulos Alexandros, et al. Fatigue assessment of offshore wind turbines on monopile foundations using multi-band modal expansion. Wind Energy 2017;20(8):1463–79.
[25] Cui Weicheng. A state-of-the-art review on fatigue life prediction methods for metal structures. J Mar Sci Technol 2002;7:43–56.
[26] Stephens Ralph I, et al. Metal fatigue in engineering. John Wiley & Sons; 2000.
[27] CEN. Eurocode 1993-1-9: Design of steel structures, Part 1.9: Fatigue. In: European committee for standardisation. 2003.
[28] Palmgren A. Die lebensdauer von kugellagern. z. vdi 68. 1924, p. S339–S341.
[29] Miner Milton A. Cumulative damage in fatigue. 1945, p. A159-A164.
[30] Myers Raymond H, Montgomery Douglas C, Anderson-Cook Christine M. Response surface methodology: Process and product optimization using designed experiments. John Wiley & Sons; 2016.
[31] García-Macías Enrique, et al. An innovative methodology for online surrogate-based model updating of historic buildings using monitoring data. Int J Archit Herit 2021;15(1):92–112.
[32] Deng Lu, Cai CS. Bridge model updating using response surface method and genetic algorithm. J Bridge Eng 2010;15(5):553–64.
[33] Gou Hongye, et al. In-situ testing and model updating of a long-span cable-stayed railway bridge with hybrid girders subjected to a running train. Eng Struct 2022;253:113823.
[34] Zhang Zesheng, Qiu Zhiping. Fatigue reliability analysis for structures with hybrid uncertainties combining quadratic response surface and polynomial chaos expansion. Int J Fatigue 2021;144:106071.
[35] Abdelmoety Ahmed K, et al. Strain-based reliability analysis of dented pipelines using a response surface method. J Pipeline Sci Eng 2022;2(1):29–38.
[36] Inzunza-Aragón Indira, Ruiz Sonia E, Cruz-Reyes Laura. Use of artificial neural networks and response surface methodology for evaluating the reliability index of steel wind towers. Adv Civ Eng 2022;2022.
[37] Han Zhong-Hua, et al. Surrogate-based optimization. In: Real-world applications of genetic algorithms. 2012, p. 343.
[38] Jiang Ping, Zhou Qi, Shao Xinyu. Surrogate model-based engineering design and optimization. Berlin/Heidelberg, Germany: Springer; 2020.
[39] MIDAS Gen© & Midas FEA NX©, MIDAS Information Technology Co.
[40] Bouzas O, et al. A holistic methodology for the non-destructive experimental characterization and reliability-based structural assessment of historical steel bridges. Eng Struct 2022;270:114867.
[41] Douglas Bruce M, Reid Wayne H. Dynamic tests and system identification of bridges. J Struct Div 1982;108(10):2295–312.
[42] Carmelo Gentile. Modal and structural identification of a RC arch bridge. Struct Eng Mech 2006;22(1):53–70.
[43] Carmelo Gentile, Saisi A. Ambient vibration testing of historic masonry towers for structural identification and damage assessment. Constr Build Mater 2007;21(6):1311–21.